Received: 6 October 2020 | Revised: 3 June 2021 | Accepted: 7 June 2021 | Published on: 18 June 2021

DOI: 10.1002/joc.7248

RESEARCH ARTICLE

International Journal of Climatology RMetS

Differences in tornado activities and key tornadic environments between China and the United States

Ruilin Zhou[1] | **Zhiyong Meng**[1] | **Lanqiang Bai**[2]

[1]Department of Atmospheric and Oceanic Sciences, School of Physics, Peking University, Beijing, China

[2]School of Atmospheric Sciences, Sun Yat-sen University, Zhuhai, China

Correspondence
Zhiyong Meng, Department of Atmospheric and Oceanic Sciences, School of Physics, Peking University, Beijing 100871, China.
Email: zymeng@pku.edu.cn

Funding information
National Natural Science Foundation of China, Grant/Award Numbers: 41875051, 41905043, 42030604

Abstract

The yearly tornado occurrence in China is approximately 5–10% of that in the United States, and the peak month of tornado occurrence in China is July, while that in the United States is May. However, the two countries have nearly the same land area and similar latitudinal location. This study attempts to disclose the differences in the key tornadic environments that are most possibly responsible for the large discrepancy of tornado occurrences observed between the two countries. The region with the highest tornado density in China (JS) is compared with three similarly sized regions in the United States, including two tornado-prone regions (UC and USE1) and one region similar to JS (USE2). The results show that JS has a much lower tornado frequency than UC and USE1, mainly due to JS's much lower likelihood of multiple tornadoes occurring in a short period during its tornado season. Compared with UC and USE1, JS features relatively low mean values of the significant tornado parameter (STP) during their respective tornado seasons. The STP, incorporating several tornado-related variables, was found to show a monotonic relationship with the total tornado count at a seasonal scale and perform well to explain monthly variations in tornado frequencies. Compared with the target regions in the United States, JS has a similar magnitude and decreasing trend of the 0–6-km vertical wind shear from spring to summer, but a later increase in instability. Resulting from a balance between the decreasing vertical shear and the increasing thermodynamic instability, JS features a delayed monthly peak of STP and thus a delayed tornado season, which makes JS having a worse kinematic environment for tornadogenesis with far lower low-level vertical wind shear during its tornado season than that of the United States.

KEYWORDS

China, difference, environmental features, significant tornado parameter, tornado, the United States

1 | INTRODUCTION

Tornado occurrence in the United States is significantly higher than that in other regions in the world (Brooks *et al*., 2003; Farney and Dixon, 2015). Based on the tornado database from NOAA's Storm Prediction Centre, the average annual number of U.S. tornadoes in the last three decades was approximately 1,200 and tornadoes were most active in the United States in May. Despite China's similar latitudinal location and land area, the

annual tornado count in China is less than one-tenth that in the United States, and the peak number of tornadoes occurs 2 months later in China than in the United States (Fan and Yu, 2015; Chen *et al*., 2018). The factors that cause tornado activities to be so different between the two countries remain unclear. This study aims to disclose the differences in the key tornadic environments that are most possibly responsible for the large tornado occurrence discrepancy between China and the United States.

Tornadoes tend to form in environments with substantial low-level shear, in addition to moisture, instability and vertical motion, which are the three ingredients of deep moist convection (Brooks *et al*., 2003; Grams *et al*., 2012; Anderson-Frey *et al*., 2018). Many proximity sounding studies have indicated that favourable tornadic environments tend to have low values of the lifted condensation level (LCL), which is correlated with high environmental humidity at low levels (Grams *et al*., 2012; Thompson *et al*., 2012). Instability, which is often measured by convective available potential energy (CAPE) and released by large-scale vertical motion, is essential for speeding up the surface air parcel vertically during deep convection (Emanuel, 1994). Compared with other convective modes, supercell thunderstorms are characterized by deep and persistent rotating updrafts, which seem to have a stronger ability to produce tornadoes (Duda and Gallus, 2010). In addition to the thermodynamic parameter of moisture and instability, the kinematic parameter of the 0–6-km vector shear magnitude (SHR6), which is important for the development of the midlevel rotation of the mesocyclone in a supercell through the tilting of its associated horizontal vorticity by a storm-scale updraft, is often used to assess the potential of supercells (Rasmussen and Blanchard, 1998; Thompson *et al*., 2003). The combination of the CAPE and SHR6 parameters has been shown to be effective in discriminating between severe and nonsevere thunderstorms (Brooks *et al*., 2003; Taszarek *et al*., 2017), and the CAPE–SHR6 parameter space is often investigated to offer valuable insight into tornadic environments (e.g., Brooks, 2009; Grünwald and Brooks, 2011; Anderson-Frey *et al*., 2016).

Low-level environmental storm-relative helicity (SRH) also provides a good reference for the development of low-level rotating updrafts and thus the potential for tornadogenesis (Kerr and Darkow, 1996; Davies-Jones, 2015; Coffer *et al*., 2019). SRH is calculated by integrating the multiplication of the storm-relative velocity vector and the streamwise vorticity from the ground to some selected height (Davies-Jones *et al*., 1990). In an environment with a large low-level SRH value, where lower-tropospheric horizontal streamwise vorticity is more dominant than lower-tropospheric horizontal crosswise vorticity, the horizontal vortex tubes are more inclined to be tilted and stretched into strong near-surface vertical vorticity (Nowotarski and Jensen, 2013; Markowski and Richardson, 2014).

Although tornadogenesis is ultimately dependent on smaller-scale processes, it has long been known to be closely related to large-to-mesoscale environments. Such large-to-mesoscale environments are often depicted by the four environmental parameters described above, namely, CAPE, SHR6, LCL and SRH (e.g., Rasmussen and Blanchard, 1998; Rasmussen, 2003; Potvin *et al*., 2010; Anderson-Frey *et al*., 2016). These environmental parameters are accounted for in the STP (Thompson *et al*., 2003), which was developed to discriminate significant tornadic environments from non-tornadic environments and has been widely used for operational tornado forecasts (Thompson *et al*., 2012). The nondimensional energy-helicity index (EHI), which combines CAPE with low-level SRH, is also commonly employed as a means of identifying tornado potential (Hart and Korotky, 1991; Rasmussen, 2003). To date, it remains unclear how these tornado-favourable environmental parameters differ between China and the United States.

Tornado frequency has been demonstrated to be correlated with monthly to seasonal environmental features. An empirical index based on monthly averaged convective precipitation and SRH has been demonstrated as having some skill in accounting for monthly tornado counts in the United States (Tippett *et al*., 2012; Tippett *et al*., 2014). The observed shift in the seasonality of tornado reports over the Great Plains has been accompanied by corresponding trends in an environmental index that is a function of CAPE and SRH (Lu *et al*., 2015). In addition, the sum of the daily maximum of the STP shows consistent changes in its spatial distribution with the tornado frequency in the United States at monthly and seasonal scales, and the spatial dependence of tornado frequency on the STP was found to vary seasonally (Gensini and Brooks, 2018; Gensini and Bravo de Guenni, 2019). These results imply that understanding the environmental differences in tornado-prone months may be a key perspective for understanding the differences in frequency of tornadoes and the monthly variations in tornadoes between China and the United States.

In the present study, tornado records from 2007 to 2016 were collected to reveal key environmental factors that may have made tornadoes in China considerably less frequent and occurring 2 months later than those in the United States. To achieve these goals effectively and efficiently, special attention was primarily paid to high-incidence tornado regions and to the prime months of tornado occurrence. The rest of the paper is organized as follows. Section 2 introduces the data and methods. The

results are presented in Section 3, followed by a discussion in Section 4 on typical synoptic situations, the potential impact of topography and some study limitations. Section 5 gives a brief summary.

2 | DATA AND METHODS

2.1 | Tornado databases

The tornado information for contiguous China from 2007 to 2016 was obtained from various sources with cross-checking, including the Yearbook of Meteorological Disasters in China (China Meteorological Administration, 2005–2017), the tornado dataset covering contiguous China during the period 1948–2012 compiled by Chen *et al.* (2018), almost all the published papers on tornadoes in China, the damage surveys conducted by local meteorological agencies and the reports archived through web searches. Quality control of the tornado records was performed by reviewing the national and regional radar reflectivity mosaic images (available at http://data.cma.cn/en), and tornado records that were not associated with a convective storm were removed.

We defined the study period as 2007–2016 for two main reasons. First, the tornado data collected in these years have much less uncertainty than those collected before 2007. Because the China New Generation Weather Radar (CINRAD) network began to take shape after 2006, we were able to perform quality control on tornado records with the availability of radar reflectivity mosaic images during the chosen study period. With the wide use of smart phones since 2007, far fewer tornado reports should have been missed. Second, this study aims to discuss the environmental parameters behind the large differences in the total number of tornadoes between China and the United States rather than the climatological variability associated with the tornado counts. The high-incidence areas and prime months of tornadoes revealed from these 10-year data are consistent with those determined in previous studies with longer study periods in both China (Chen *et al.*, 2018) and the United States (e.g., Ashley, 2007; Tippett *et al.*, 2012). Consequently, using the 10-year data from 2007–2016 should be reasonable for this study.

A total of 983 tornado reports were catalogued in China from 2007 to 2016. This tornado dataset has been made available at the Peking University Open Research Data Platform at https://doi.org/10.18170/DVN/QKQHTG (Zhou *et al.*, 2020). The tornado information over the same period in the contiguous United States was derived from NOAA's Storm Prediction Centre (SPC) severe weather database (available at https://www.spc.noaa.gov/wcm/#data), which has been used widely in the literature. During the 10 studied years, a total of 11,795 tornadoes were catalogued in the United States, which is approximately 12 times the number recorded in China.

2.2 | Selection of target regions

To achieve our goals, we focused on regions with high frequency of tornadoes. Figure 1a,b shows that most tornadoes occur in eastern China, with the highest tornado frequency occurring in Jiangsu Province (the red box in Figure 1a), where the terrain is generally flat. We thus selected a region of interest confined by the area within 31–35°N and 118–122°E (4° × 4°) and labelled this region as JS. In the United States, the highest tornado frequency is located in the region to the east of the Rocky Mountains. We chose the 4° × 4° area confined by 36–40°N and 97–101°W as the high-incidence region and labelled it UC; this region is located in the central and southern Great Plains of the United States (Figure 1c,e).

In addition to the central and southern Great Plains, Mississippi and Alabama, which are located in the southeastern United States, have the second-highest tornado frequencies in the United States and have been confirmed to be the two states that hold the highest tornado fatality rates other than Arkansas (Ashley, 2007; Coleman and Dixon, 2014). Thus, we chose the 4° × 4° area within 31–35°N and 86–90°W (Figure 1c,f) as another high-incidence region in the United States and labelled this region as USE1. We further chose the 4° × 4° area within 32–36°N and 78–82°W as USE2 (Figure 1c,d) to create a target region in the United States that roughly matches JS in China in terms of a similar tornado count, latitude, terrain elevation and location relative to a coastline.

2.3 | Environmental parameters

The long-term spatial means of relevant environmental parameters can be used to represent the overall environmental features of the four target regions in a statistical sense. The environmental parameters were calculated using the National Centres for Environmental Prediction Final Operational Global Analysis dataset (NCEP FNL, available online at https://rda.ucar.edu/datasets/ds083.2/) with a 6-hr interval and 1° × 1° horizontal resolution. In the calculations of atmospheric parameters, only NCEP FNL data over the grid points located on land or near the coast were used (Figure 1b,d) for two main reasons. First, there are almost no tornado reports over the ocean in the northeast corner of JS or in the southeast corner of USE2. Waterspouts over oceans have little chance of being

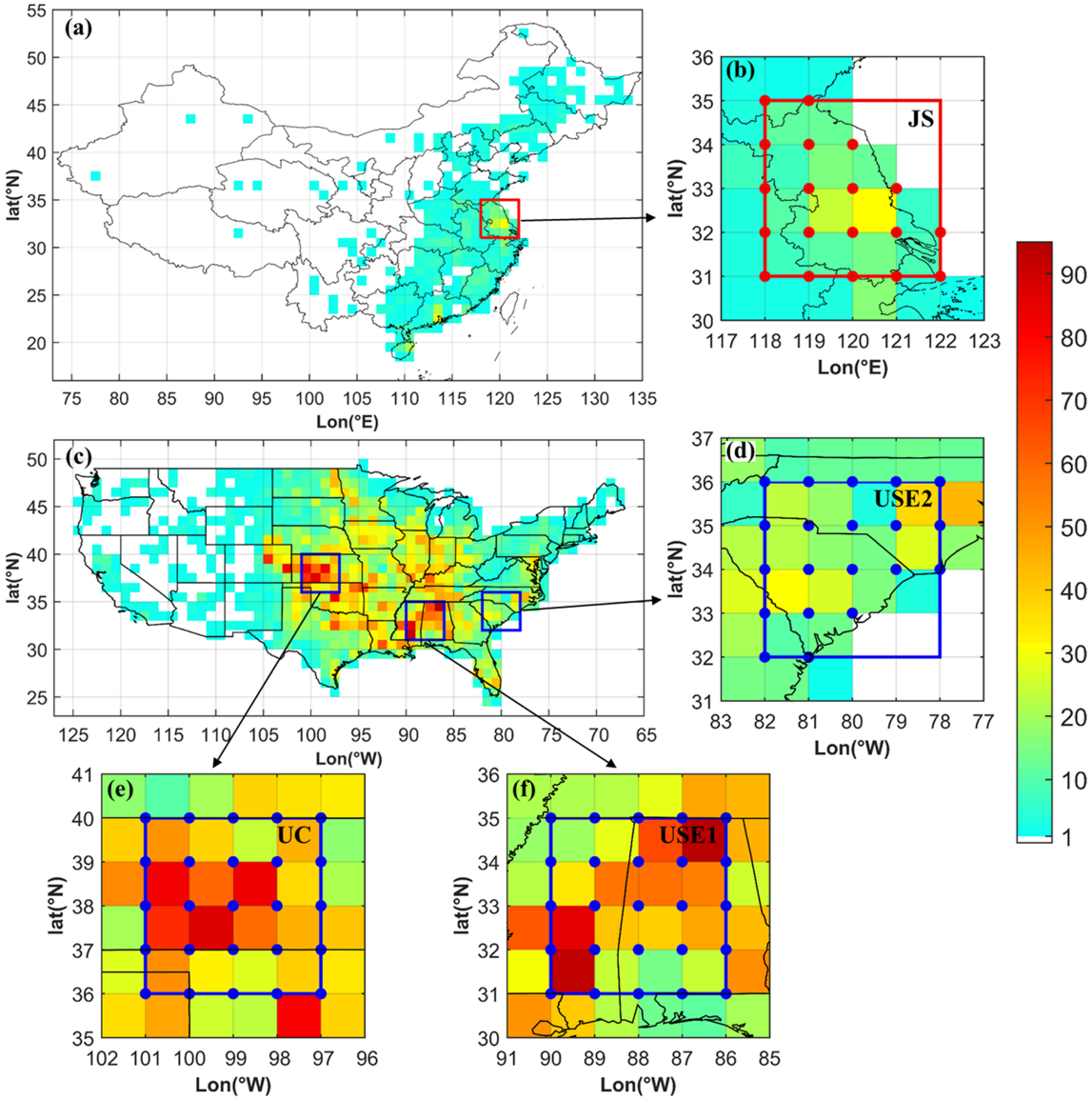

FIGURE 1 (a) Spatial distribution of tornado occurrences in contiguous China from 2007 to 2016 displayed on 1° × 1° latitude–longitude grids. The region in the red box is enlarged in (b). The red dots in (b) denote the locations where the NCEP FNL data were used to calculate environmental features. (c) As in (a) but for the tornadoes that occurred in the contiguous United States during the same period. (d)–(f) Same as in (b) but corresponding to the selected target regions in the United States, namely, USE2, UC, and USE1 (indicated by the blue boxes and black arrows). NCEP FNL data over the blue grid points in (d)–(f) were used to calculate environmental features. The colour bar is employed for (a)–(f)

detected and are difficult to verify due to insufficient radar coverage and impractical damage surveys. Additionally, the boundary layer conditions over the ocean are substantially different from those over land, which would affect the derived convective parameters examined in this study.

Several tornado-related atmospheric parameters were composited over the studied spatial and temporal ranges for the four target regions during the tornado-prone months: 0–1-km SRH (SRH1), mixed-layer CAPE (MLCAPE), SHR6, mixed-layer LCL (MLLCL), STP and EHI. MLCAPE was calculated using a parcel lifted from a mixed layer in the lowest 100 hPa. In calculating SRH1, the storm motion was estimated using the method of Bunkers *et al.* (2000). The STP was calculated following the process of Thompson *et al.* (2003) using a mixed-layer method (also within the lowest 100 hPa).

$$\mathrm{STP} = \left(\frac{\mathrm{MLCAPE}}{1000\,\mathrm{J\,kg^{-1}}}\right) \times \left(\frac{2000\,\mathrm{m} - \mathrm{MLLCL}}{1500\,\mathrm{m}}\right) \times \left(\frac{\mathrm{SRH1}}{100\,\mathrm{m^2\,s^{-2}}}\right) \times \left(\frac{\mathrm{SHR6}}{20\,\mathrm{m\,s^{-1}}}\right).$$

EHI was calculated according to the modified version outlined in Rasmussen (2003).

$$\mathrm{EHI} = \frac{\mathrm{MLCAPE} \times \mathrm{SRH1}}{160000}.$$

These atmospheric parameters were first calculated for every 6-hr data time series for the grid points located on land or near the coast in each of the four target regions. The values of these environmental parameters on grids within 1,000 km of a tropical cyclone (TC) centre during the period affected by TCs were removed to eliminate the influences of TCs on the environmental characteristics. These atmospheric parameters were then averaged in each of the four regions throughout their respective tornado-prone months to obtain mean values.

The tropical cyclone best-track data were obtained from the HURDAT2 database (Landsea and Franklin, 2013, available online at https://www.nhc.noaa.gov/data/hurdat/) and the database compiled by Regional Specialized Meteorological Centre Tokyo (RSMC, available online at http://www.jma.go.jp/jma/jma-eng/jma-center/rsmc-hp-pub-eg/besttrack.html).

2.4 | Tornado event and its tornado-generating efficiency

Tornado outbreaks often occur in the United States but are rare in China. A tornado outbreak event is generally described as the occurrence of 10 or more tornadoes associated with the same synoptic-scale storm system (Galway, 1977; Glickman, 2000). In our attempts to seek the causes of the different tornado numbers observed between the four target regions, it is important to take into account the frequency with which multiple tornadoes occur in a short period and measure the effects of this type of occurrence on the total tornado counts.

In this work, tornadoes that occur at close times and locations are considered one tornado event. The tornado event dataset is built as follows.

1. For each tornado, a corresponding tornado event is determined to include this tornado and the tornadoes that occur in its proximity within 6 hr and within a $1^\circ \times 1^\circ$ region relative to this tornado. The initial set of the number (Nt) of tornadoes that occur in a tornado event is then obtained. This dataset is labelled the 'old' tornado event dataset, and it contains many duplicate tornado reports.
2. The tornado event with the largest Nt in the 'old' dataset is selected and moved from the 'old' dataset to the 'new' dataset. Tornado events with the same Nt values are processed in chronological order. The tornado reports that occur in this tornado event are identified and removed from the remaining tornado events in the 'old' dataset. For the 'old' dataset, the Nt values for all tornado events are then updated, and the tornado events with Nt = 0 are removed.
3. The second step is repeated until the 'old' dataset is empty.
4. These tornado events in the 'new' dataset are then used for the following analysis.

To assess the potential for multiple tornadoes to occur in a short period in a given region, the tornado-generating efficiency of tornado events is defined as the number of total tornado reports (Ntor) divided by the number of total tornado events (Nte), which reflects the average number of tornadoes that occur per tornado event. It should be noted that this definition of the tornado-generating efficiency of tornado events mostly considers the tornado number and does not include information such as the durations, path lengths or intensities of tornadoes. In this study, an efficient tornado event does not indicate a long-lived, long-tracked or severe tornado event.

3 | RESULTS

3.1 | Tornado activity

The characteristics of tornado activities in JS and UC, the regions with the highest tornado frequencies in China and the United States, respectively, are examined first. As shown in Figure 2a, JS has a similar temporal distribution of tornadoes to that of all of China, which is possibly due to the much higher frequency of tornadoes in JS than in other regions, including in the southern part of China. The same is also true for UC relative to the contiguous United States (Figure 2a). Considering that their highest tornado densities and monthly variations in tornado number are similar to those of the whole country, UC and JS can be used as representative areas of the United States and China, respectively. Figure 2a shows that there are also some tornadoes that occur in April and May in China, most of which are located in the southern part of China (Chen *et al*., 2018). Southern China is not the focus of this study due to its mountainous terrain and its relatively low tornado density (Figure S1).

To analyse the most representative environmental characteristics of different regions at the same time scale, we defined the tornado season of each region as the three consecutive months from the month before to the month

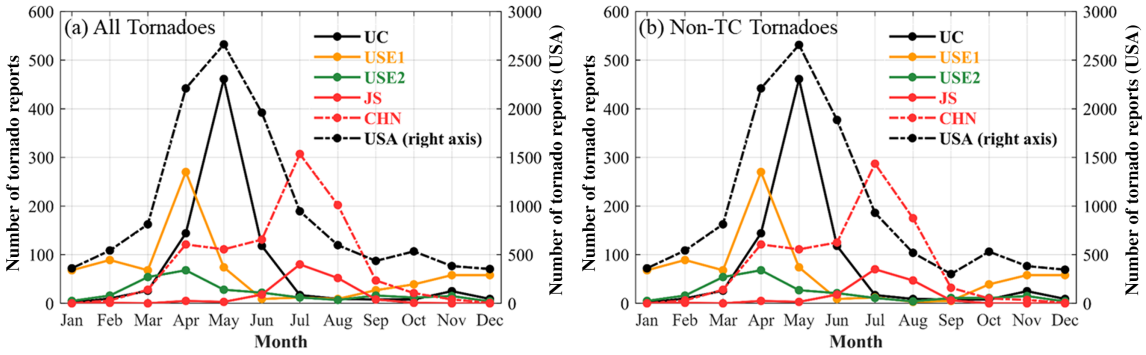

FIGURE 2 Monthly distributions of all tornadoes (a) and non-TC tornadoes (b) from 2007 to 2016 in the four target regions (shown by the left axis), contiguous China (CHN; shown by the left axis) and the United States (USA; shown by the right axis)

after the month of peak tornado occurrence. JS has a peak tornado occurrence in July (Figure 2a) with a tornado season from June to August. In the UC area of the United States, the tornado season lasts from April to June, with the most active month in May (Figure 2a). Meanwhile, both USE1 and USE2 have a tornado season from March to May (Figure 2a).

Although some tornadoes are known to occur in association with TCs, this work focuses only on tornadoes that are not associated with TCs. TC tornadoes are identified within 1,000 km of the centre of their parent TCs (McCaul, 1991). As shown in Figure 2b, TC tornadoes have little effect on the timing of tornado seasons or on the tornado numbers in the four target regions. The results show that TC tornadoes tend to prevail in the southeastern United States from July to September. During the tornado seasons throughout the 10 studied years, no TC tornado was observed in UC or USE1, and only one TC tornado was identified in USE2 in May 2012. In JS during its tornado seasons, TC tornadoes account for only 10% of the total tornadoes, including four Nt > 1 TC tornado events, although JS constitutes a spatial peak of TC-associated tornadoes in China (Bai *et al.*, 2020). For a consistent comparison, the TC tornadoes were removed from the following discussion, if not otherwise stated.

During the tornado season in JS, a total of 135 non-TC tornadoes were recorded from 2007 to 2016, accounting for 23% of all reported non-TC tornadoes in China from June to August in this period. In comparison, there are 723 non-TC tornadoes recorded in UC during its tornado seasons from 2007 to 2016, accounting for 10.7% of all reported non-TC tornadoes in the United States in the same period; this value exceeds the number of tornadoes that were recorded in JS during its tornado seasons by five times.

The results show that a large difference in the potential for multiple tornadoes to occur within a short period exists between JS and UC in their respective tornado seasons. The number of Nt > 1 tornado events in JS is much smaller than that in UC, while the number of Nt = 1 tornado events in JS is close to that in UC (Figure 3a). A total of 100 non-TC tornado events were identified in JS during its tornado seasons (June–August) throughout the study period, including 78 tornado events of Nt = 1 and 22 tornado events of Nt > 1 (Figure 3a). Meanwhile, 169 tornado events were identified in UC, with 72 tornado events of Nt = 1 and 97 tornado events of Nt > 1 recorded during its tornado seasons (April–June) throughout the study period (Figure 3a). In UC, the monthly distribution of all tornado events is similar to that of Nt > 1 tornado events, with the peak month dominated by Nt > 1 tornado events (Figure 4a,c). In contrast, the Nt = 1 tornado events dominate in JS (Figure 4b,c).

The difference in the number of tornado events of Nt > 1 determines the difference in the total tornado count between JS and UC. Figure 3b shows that 90% of tornadoes in UC are characterized by Nt > 1 tornado events, while the majority (57.8%) of tornadoes in JS correspond to Nt = 1 tornado events. The difference in the total tornado count between JS and UC is more obvious for high-Nt tornado events. A total of 51 tornado events of Nt > 4 contribute to nearly three-quarters of the tornado reports in UC, while there is only one case of Nt > 4 recorded in JS (not shown).

Similar to UC, outstanding contributions of tornado events of Nt > 1 to the total tornado counts were also observed in USE1 and USE2 (Figure 3b). During the tornado seasons (March–May), more than 80% of the total tornado counts were attributed to tornado events of Nt > 1 in USE1 and USE2. Figure 3a,b shows that the main difference in the total tornado count between USE1 and JS comes from tornado events of Nt > 1. Even though USE2 has far fewer tornado events of Nt = 1 and a slightly greater number of Nt > 1 tornado events than

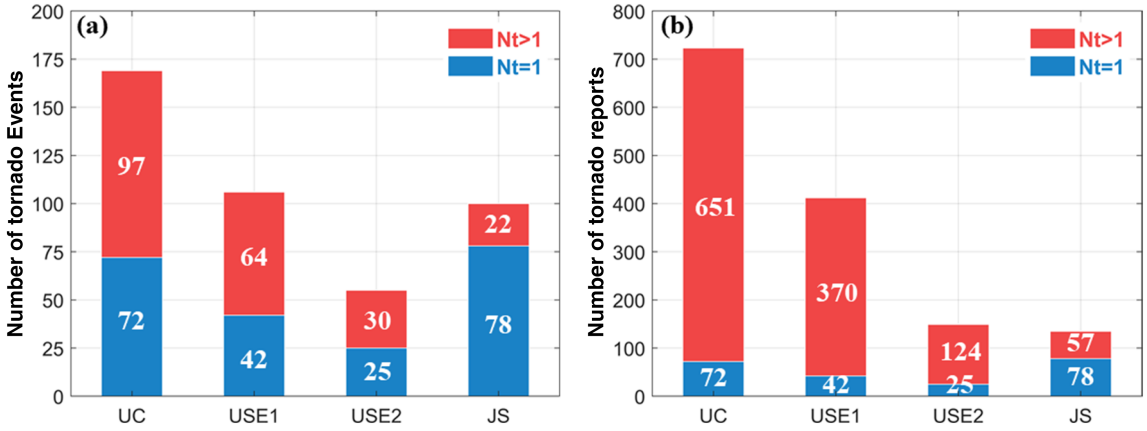

FIGURE 3 (a) Numbers of Nt > 1 (red) and Nt = 1 (blue) non-TC tornado events in the four target regions during their respective tornado seasons (UC, April to June; USE1, March to May; USE2, March to May; JS, June to August). (b) As in (a), but for the numbers of tornado reports from Nt > 1 non-TC tornado events (red) and Nt = 1 non-TC tornado events (blue)

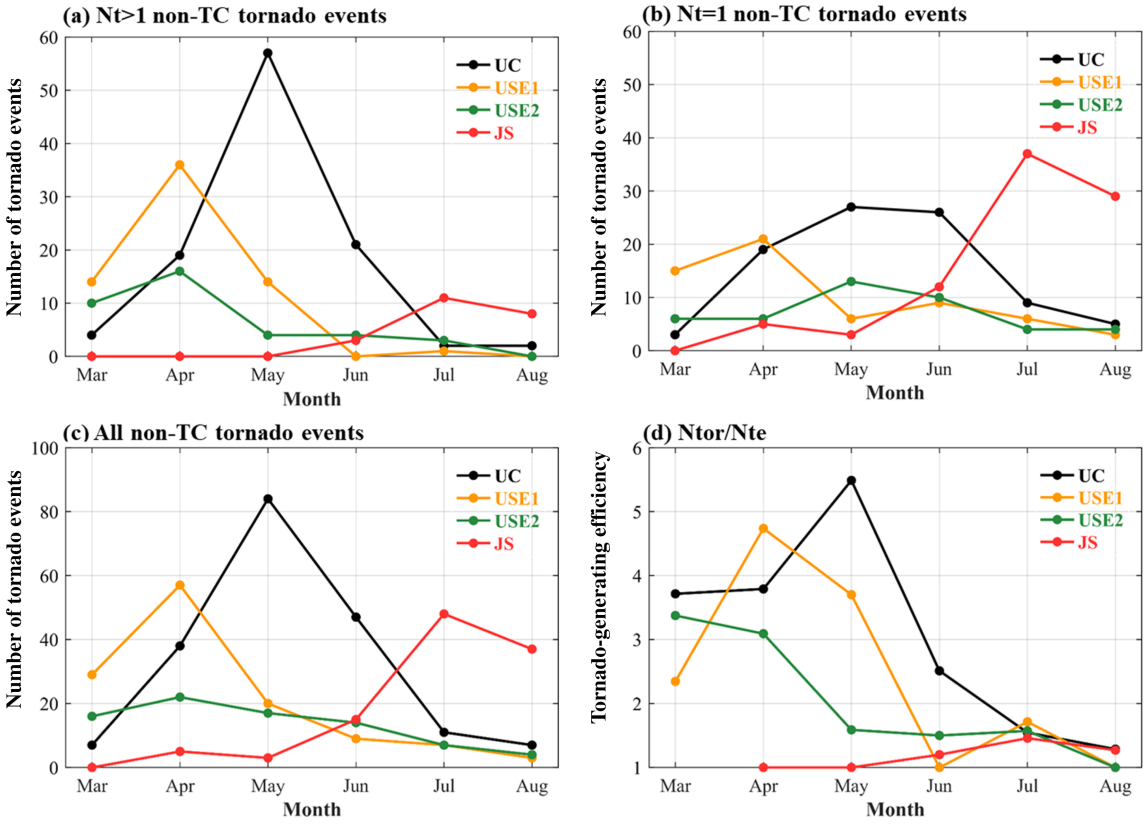

FIGURE 4 Monthly distributions of Nt > 1 non-TC tornado events (a), Nt = 1 non-TC tornado events (b), all non-TC tornado events (c), and tornado-generating efficiency of tornado events (d) from 2007 to 2016 in the four target regions

JS, the higher likelihood of high-Nt tornado events in USE2 (10 Nt > 4 cases in USE2) helps it to exceed JS in terms of their total tornado numbers.

In agreement with the numbers and proportions of Nt > 1 tornado events (Figure 3a), the tornado-generating efficiency of tornado events (Ntor/Nte) decreases monotonically from UC (4.28) to USE1 (3.89), USE2 (2.71) and JS (1.35) during their corresponding tornado seasons, indicating the decreasing likelihood of multiple tornadoes occurring during a single event in

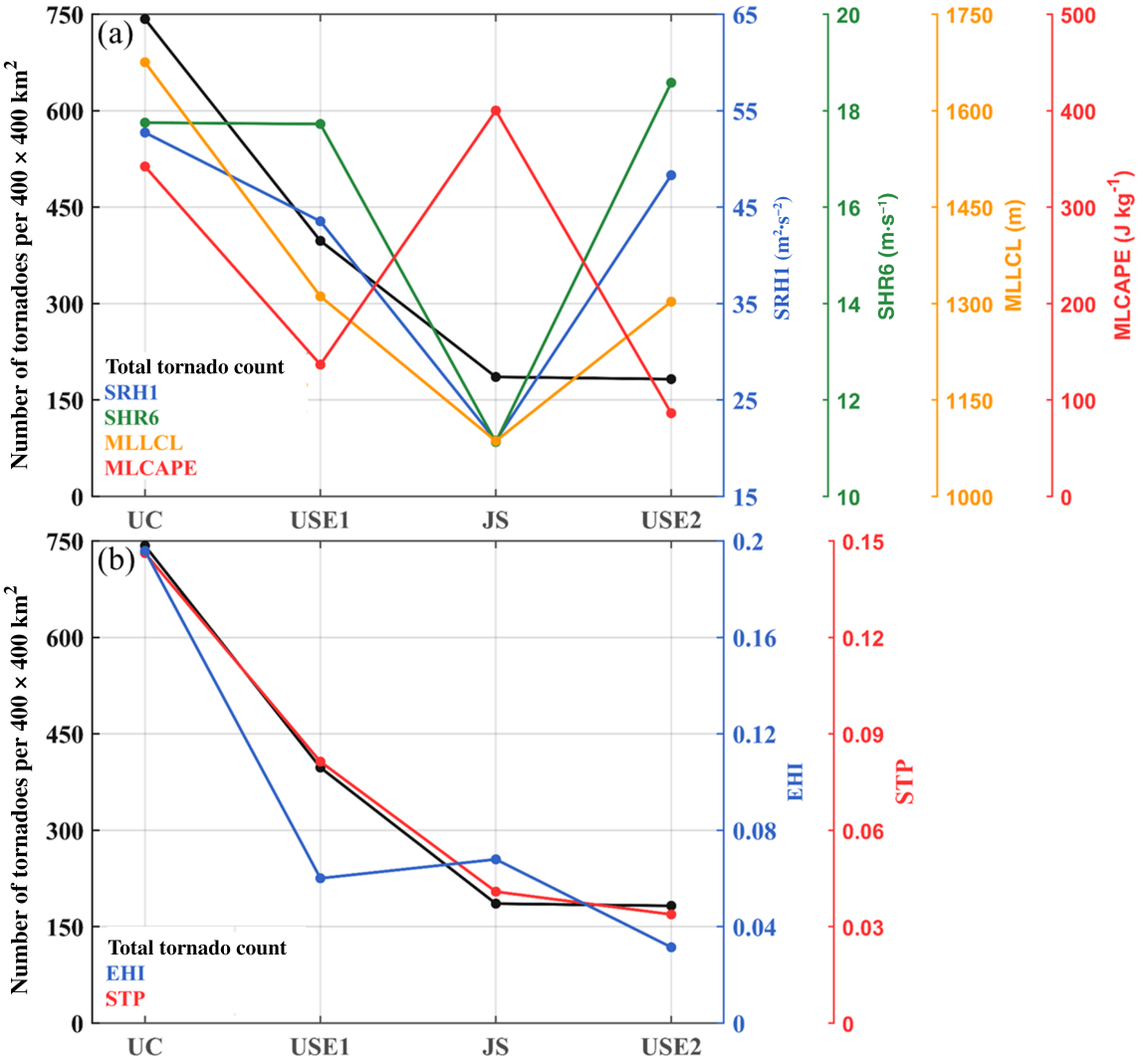

FIGURE 5 (a) The area-scaled total tornado counts (shown by the left axis) and the average SRH1, SHR6, MLLCL and MLCAPE values (shown by the right axis) in the four target regions during their respective tornado seasons. (b) The area-scaled total tornado counts (shown by the left axis) and the average composite indices EHI and STP (shown by the right axis) in the four target regions during their respective tornado seasons

these regions. However, this feature fails to be maintained outside of the tornado season. In the three target regions of the United States, the tornado-generating efficiency of tornado events declines obviously in summer and becomes similar to that of JS in July and August (Figure 4d), with fewer occurrences of Nt > 1 tornado events in summer than in spring (Figure 4a). Nt = 1 tornado events become more common in summer than Nt > 1 tornado events (Figure 4a,b).

3.2 | Environmental features related to total tornado counts

To accurately describe the tornado density with respect to area, we divided the total tornado count in each region by the area of the region. As shown in Figure 1b,d, both the northeast corner of JS and the southeast corner of USE2 cover some ocean areas, where almost no tornadoes were recorded. Latitudinal differences also contribute to the differences in the land area. The actual land areas of UC, USE1, USE2 and JS are 155,785, 165,819, 130,620 and 116,195 km^2, respectively. The total tornado count in each of the four target regions is scaled by its land area and converted to an amount per 400 × 400 km^2 hereafter, if not otherwise stated. Figure 5a,b shows that the area-scaled total tornado counts decrease from UC (743) to USE1 (398), JS (186) and USE2 (183) during their corresponding tornado seasons.

To examine the main environmental factors that affect the area-scaled total tornado counts, the average values of several tornado-related parameters were

calculated for each of the four regions throughout their respective tornado seasons using the method described in Section 2.3.

The target regions in the two countries are noticeably differentiated by their environmental features during their respective tornado seasons. In the JS region of China, the kinematic environment is unfavourable for tornadoes and supercells, with low mean values of SRH1 and SHR6, while the thermodynamic conditions seem to be conducive to the occurrences of severe storms, with relatively high MLCAPE and low MLLCL values (Figure 5a). Compared with JS, UC is characterized by a more favourable kinematic environment with higher SRH1 and SHR6 values but is also characterized by a drier environment with a higher MLLCL value (Figure 5a). USE1 and USE2 have similar environments with high SHR6 but low CAPE values (Figure 5a). The phenomenon in which many tornadoes occur in high-shear but low-CAPE environments in the southeastern United States has gradually received more significant attention recently (e.g., Sherburn and Parker, 2014; Long *et al*., 2018; Brown and Nowotarski, 2020).

Relative to the absence of consistent variation observed between a particular kinematic or thermodynamic parameter alone and the total tornado count, the composite index STP shows a consistent change with the monotonic decrease in the area-scaled total tornado count from UC to USE1, JS and USE2 (Figure 5b). UC has a much higher STP value with a much higher total tornado count than the other target regions, followed by USE1 with the second-highest total tornado count. JS and USE2 have similar STP averages, which is consistent with their comparable total tornado counts. Although the EHI is also a composite parameter of both kinematic and thermodynamic factors similar to the STP, it performs worse than the STP in assessing the total tornado count of a given region (Figure 5b).

To verify the effect of the STP on the total tornado count, we calculated Spearman's rank correlation coefficient (Spearman's ρ; Kendall and Gibbons, 1990), which assesses how well the relationship between two sets of data can be described using a monotonic function. The *p*-value was obtained for testing the hypothesis that there is no correlation between the two data sets against the alternative hypothesis of a nonzero correlation. The STP averages and the total tornado counts were obtained for each target region during the corresponding tornado season in each year of the 10-year study period, providing a sample containing 40 STP averages and 40 corresponding total tornado count values. As shown in Figure 6, high total tornado count values tend to be accompanied by high STP averages. The Spearman's ρ between the 40 STP averages and 40 total tornado count values is approximately 0.83, and the corresponding *p*-value is much lower than the significance level of .05. This further confirms that the total tornado count in a given region correlates strongly with the STP, indicating that a region with a high mean STP value may have more tornado occurrences.

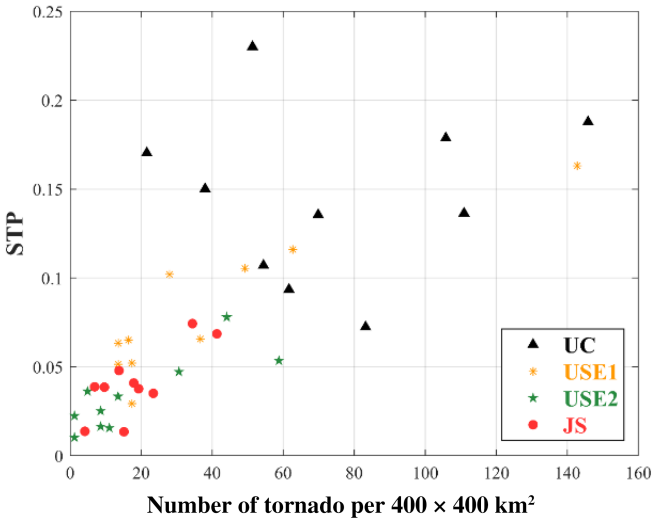

FIGURE 6 A scatter plot between the STP averages and the area-scaled total tornado counts in the four target regions during their 10 studied tornado seasons

3.3 | Environmental features related to monthly variation of tornado activity

As discussed in Section 3.1, the three target regions of the United States have many more tornadoes and relatively higher tornado-generating efficiencies of tornado events in spring than in summer, while the JS region of China has the most active tornado occurrence in summer. To explore the main environmental factors that contribute to monthly variations in tornado activity, the monthly averages of these tornado-related parameters were calculated as described in Section 2.3.

One interesting feature of SHR6 is that its mean values in the three target regions of the United States are all substantially larger than its mean value in JS (Figure 5a), suggesting that the United States may have more favourable kinematic environments for the genesis of supercells (Markowski and Richardson, 2010). Our analyses show that this is not because the United States has a generally larger SHR6 than China at any time of the year, as we speculated before. The four target regions actually have similar SHR6 values in the same months, with similar decreasing trends from March to August

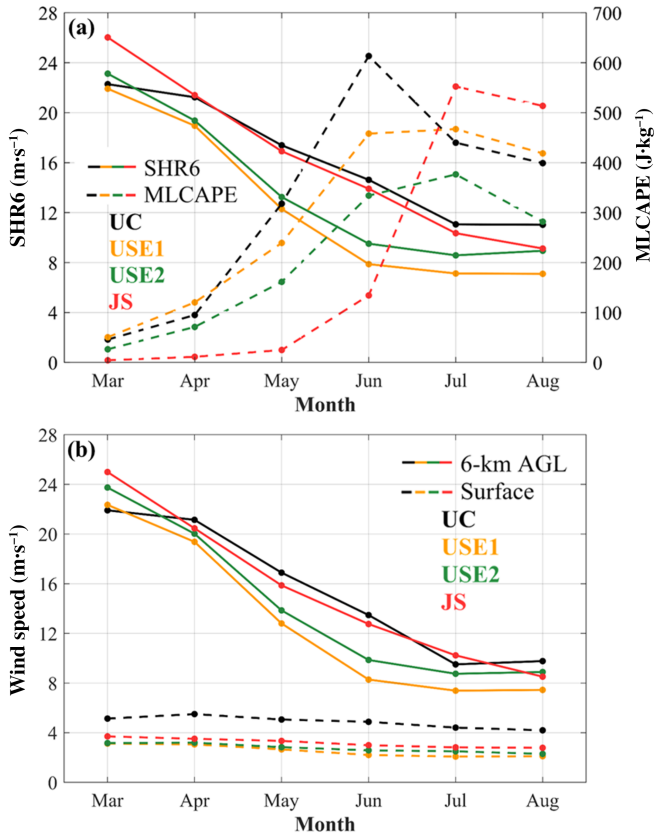

FIGURE 7 (a) Monthly variations in SHR6 (solid line; shown by the left axis) and MLCAPE (dashed line; shown by the right axis) in UC, USE1, USE2 and JS. (b) Monthly variations in wind speed at the surface (dashed line) and at an altitude of 6 km AGL (solid line) in UC, USE1, USE2 and JS

(Figure 7a). The monthly variations in SHR6 in the four target regions probably depend on changes in the magnitude of the wind at an altitude of 6 km above ground level (AGL) rather than the surface wind. The wind speeds at an altitude of 6 km AGL are usually stronger than the wind speeds at the surface, and the averaged surface wind magnitude does not change obviously from month to month (Figure 7b). In contrast, as the mid- to high-level westerlies weaken and the jet streams move poleward from spring to summer, the wind speed at an altitude of 6 km AGL in each target region shows a similar decreasing trend and similar magnitude of variation as those of SHR6 from March to August. In addition to the mean values, the box-and-whisker plot of SHR6 shows a roughly symmetric distribution with similar median and mean values (Figure 8a), demonstrating that a higher mean value is mainly contributed by a larger frequency of higher values.

The earlier tornado seasons observed in the three regions of the United States compared to that observed in JS are possibly due to the different monthly variations in instability among these target regions. The mean value of MLCAPE shows a rapid increase in UC, USE1 and USE2 but maintains a much lower value in JS from March to May (Figure 7a). Different from SHR6, the box-and-whisker plots of MLCAPE have mean values much larger than their median values, which are quite close to zero in spring (Figure 8b). A higher monthly average of MLCAPE indicates a higher frequency of strongly unstable environments in that month. In the springtime, warm and humid air is transported from the Gulf of Mexico to UC, USE1 and USE2 through the prevailing southerly flows in the lower troposphere and the strong low-level southerly jet at 925 hPa over the southern Great Plains (Feng *et al.*, 2019; Molina and Allen, 2019). In contrast, JS starts to have a large MLCAPE mean value only from June (Figure 7a). The delayed high MLCAPE values observed in JS compared with those in the U.S. locations are possibly due to the transition of baroclinic zones from South China in March and April to the mid-latitude JS region in June and July; this transition is associated with the northward propagation of the summer monsoon (Tang *et al.*, 2020). Resulting from these seasonal transitions of baroclinicity and moisture, high MLCAPE values appear in JS in summer (Figure 7a). Consequently, the three target regions of the United States reach a good match between SHR6 and MLCAPE earlier than JS, and thus have higher SHR6 values than JS in their corresponding tornado seasons.

In addition to SHR6, monthly averages of SRH1 also show an obvious decreasing trend from spring to summer in the target regions of the United States, and the averages in UC are clearly larger than those of USE1 and USE2 in May and June (Figure 9a). The JS region of China, however, has a relatively flat monthly variation in SRH1 with a small peak in July (Figure 9a). The SRH1 averages observed in JS in spring are much smaller than those in the U.S. locations but become slightly larger in July. Similar to SHR6, the SRH1 has a roughly symmetric distribution as shown in its box-and-whisker plot (Figure 8c) which also shows that the decreasing trend of monthly averaged SRH1 from spring to summer in the U.S. locations mainly results from much less occurrences of high SRH1 values greater than 100 $m^2 s^{-1}$. SRH1 measures the potential for cyclonic updraft rotation, and environments with large SRH1 values may have more streamwise vortex lines tilted upward at lower levels to form steady low-level mesocyclones that strengthen low-level updrafts to possibly trigger tornadogenesis than environments with smaller SRH1 values. The target regions in the United States have a relatively higher tornado-generating efficiency of tornado events than JS does, possibly due in part to their higher SRH1 values observed during their earlier tornado seasons; this is

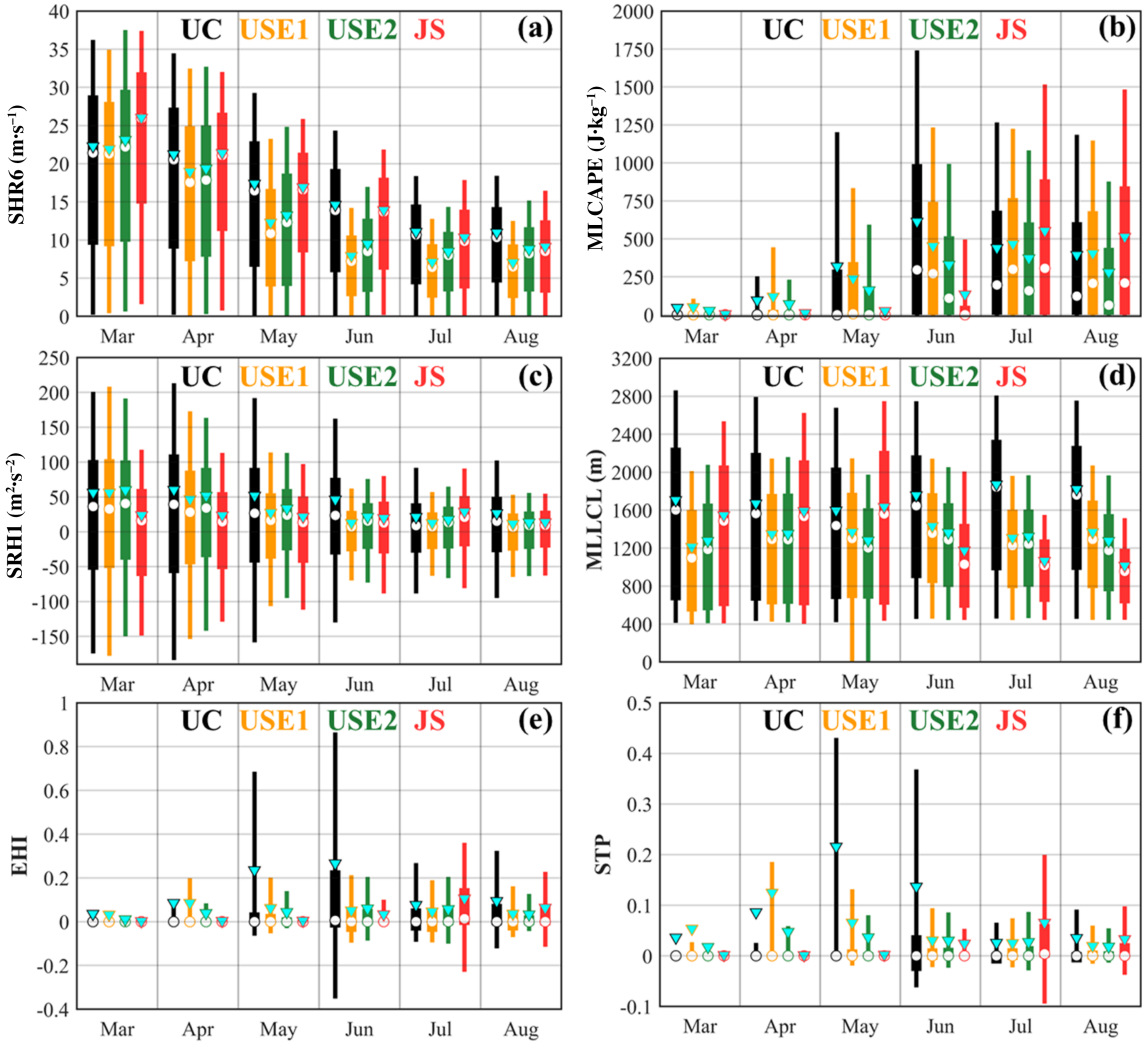

FIGURE 8 Box-and-whiskers plots of SHR6 (a), MLCAPE (b), SRH1 (c), MLLCL (d), EHI (e) and STP (f) in the four target regions from March to August during the 10 studied years. The shaded boxes span the 25th–75th percentiles, and the whiskers extend downward to the 10th and upward to the 90th percentiles. Mean values are marked by downward-pointing triangles and median values are marked by circles

consistent with the results of Anderson-Frey *et al.* (2018), who found that the SRH1 values are higher for outbreak tornadoes than for isolated tornadoes. SRH1 values are sensitive to the magnitude and orientation of low-level wind shear, as well as to the estimated storm motions. Monthly variations in SRH1 are closely related to the magnitude of the average wind speed at an altitude of 1 km AGL, which shows a similar trend from spring to summer to that of SRH1 (Figure 9a,c).

The MLLCL is greatly determined by the low-level moisture. Relative to USE1 and USE2 near the Gulf of Mexico and Atlantic Ocean, the UC region has less moisture transported from the Gulf of Mexico and is thus generally characterized by lower relative humidity at the surface and higher MLLCL than the USE1 and USE2 regions (Figure 9b,d). The increase in MLLCL observed in UC in summer possibly results from increased surface temperatures. In contrast with UC, JS has an apparent increase in relative humidity at the surface and a decrease in MLLCL from spring to summer (Figure 9b,d), benefiting from a large amount of moist air transported from the South China Sea and Indian Ocean, influenced by the summer monsoon. The tornado seasons in UC and JS correspond to the months when their MLLCL monthly mean values are relatively low (Figures 2b and 9b). As with SHR6 and SRH1, the MLLCL has a roughly symmetric distribution as shown in its box-and-whisker plot (Figure 8d).

The monthly distributions of these kinematic and thermodynamic parameters differ from each other in a given region; thus, the months in which the parameters best match should be the most favourable months for

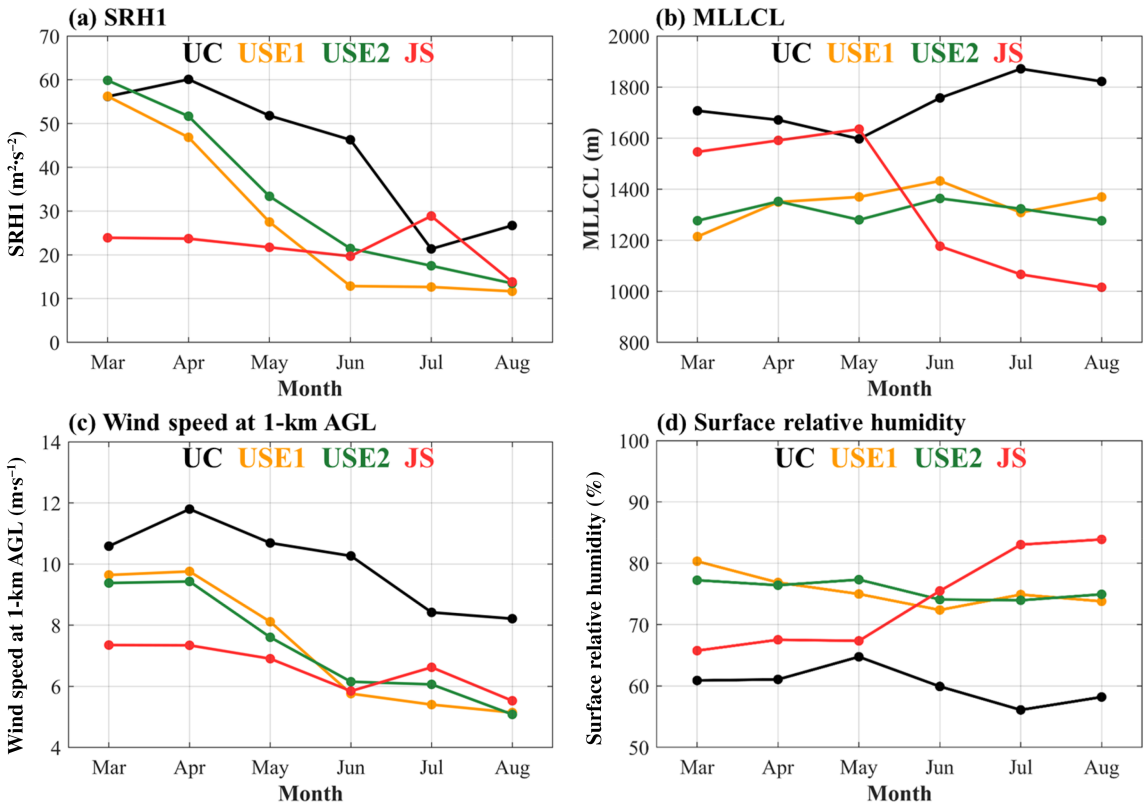

FIGURE 9 Monthly variations in SRH1 (a), MLLCL (b), wind speed at an altitude of 1 km AGL (c), and relative humidity at the surface (d) in the four target regions

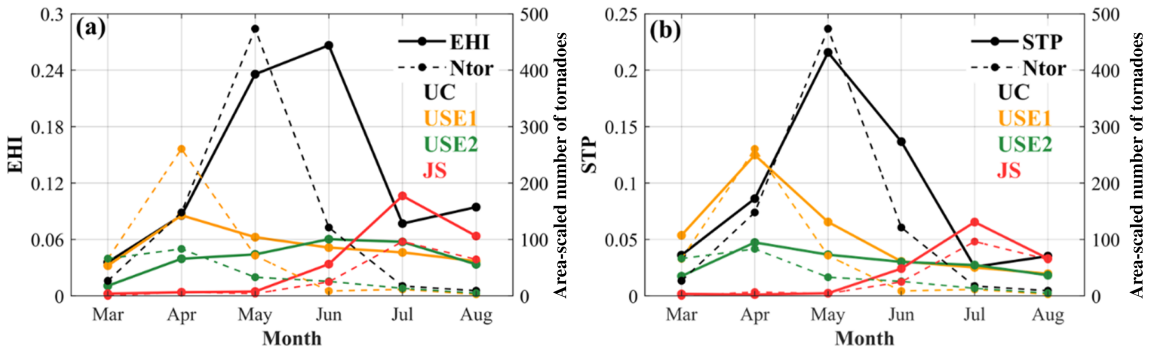

FIGURE 10 (a) Monthly variations in the EHI (shown by the left axis) and the area-scaled number of non-TC tornadoes (shown by the right axis) in the four target regions. (b) Monthly variations in the STP (shown by the left axis) and the area-scaled number of non-TC tornadoes (shown by the right axis) in the four target regions

tornadoes to occur. The configuration of these parameters was examined through the calculations of EHI and STP in this study. The results show that monthly averaged EHI shows an inconsistent trend with the monthly variations in tornado frequencies in UC and USE2, while the monthly averaged STP reflects the monthly variations in the area-scaled numbers of tornadoes in the four target regions well (Figure 10). For a given region, the peak month of the monthly averaged STP corresponds to the peak month of the area-scaled number of tornadoes (Figure 10b). Compared with the monthly averaged EHI, which only combines SRH1 and CAPE, the monthly averaged STP is a better indicator of the kinematic and thermodynamic environmental configurations associated with tornado occurrences. As with MLCAPE, but unlike SHR6, SRH1 and MLLCL, EHI and STP have mean values much larger than their median values, which are close to zero in every month (Figure 8e,f). The monthly

TABLE 1 Numbers of tornado days (Ntd), tornado events (Nte) and the ratios of Nte to Ntd in the four target regions during their respective tornado seasons

	UC	USE1	USE2	JS
Ntd	116	64	39	78
Nte	169	106	55	100
Nte/Ntd	1.46	1.66	1.41	1.28

averages of EHI and STP are greatly affected by extreme values that represent favourable kinematic and thermodynamic environments for tornadogenesis (Figure 8e,f).

4 | DISCUSSION

In the previous section, this work revealed that the different likelihoods of multiple tornadoes occurring in a short period between these target regions are most possibly responsible for their large discrepancy in tornado occurrences. The number of tornado events that occur at the same time is also of interest from the viewpoint of the synoptic control of tornadic environments. We examined the number of tornado days (Ntd) in the four target regions and the ratio of the number of tornado events (Nte) to the Ntd, which can be used to imply the approximate average number of tornado events controlled by the same synoptic situation (Table 1). The results show that the ratios of Nte in JS, UC, USE1 and USE2 to their respective Ntd are 1.28, 1.46, 1.66 and 1.41, respectively, suggesting that the U.S. regions have larger synoptic controls on their tornadic environments than the JS region, with more tornado events occurring per tornado day.

Synoptic situations have an important influence on the occurrence of severe storms. The commonly used tornado-related parameters examined in this study do not measure forcing for ascent, which is an important factor in the formation of severe storms. Large-scale upward motion forcing is often associated with apparent synoptic-scale weather systems. Rising motion is typically common ahead of a trough or near frontal systems that accompany extratropical cyclones.

To obtain a general idea of the synoptic features that are favourable for tornadoes, we examined the synoptic situations during all 22 Nt > 1 tornado events in JS and compared the typical synoptic situation in JS with those in the target regions in the United States. For each tornado event, the closest NCEP FNL data before the mean time of occurrences of all tornadoes were used. The results show that most Nt > 1 tornado events in JS occurred in front of a southwest–northeast-oriented trough at 500 hPa, with the subtropical high located in the east or southeast (Figure S3a–k). Some tornado events were mainly controlled by a short (Figure S3l–q) or a deep trough (Figure S3r–t) alone, with the subtropical high located farther to the south. The remaining two tornado events were mainly controlled by the subtropical high alone (Figure S3u–v). The upper-level jet streams move poleward and become weaker from spring to summer (Manney *et al*., 2014) and are thus located more to the north of the target area in China than those in the United States during the tornado season. Over East China, the region where tornadoes are most frequent in China, extratropical cyclones are weaker and less frequent in summer than in spring (Lee *et al*., 2019). Few Nt > 1 tornado events were found to be associated with evident surface cyclones accompanied by the upper-level jet (Figure S3n–q). Relative to JS, even though the typical patterns favourable for multiple tornadoes in U.S. locations were also mostly located in front of a deep trough or sometimes in front of a short trough, they were, however, accompanied by much stronger and wider upper-level jet streams and more intense and larger surface cyclones (Figures S4, S5 and S6). Extratropical cyclones with strong upper-level jet streams enable the production of environments that are rich in vertical wind shear in the warm sector, thus enhancing the potential of tornado outbreaks (Mercer *et al*., 2012; Tochimoto and Niino, 2016). In addition, extratropical cyclones over the United States in summer are mainly confined to relatively higher latitudes than those in spring (Wernli and Schwierz, 2006). As a result, the frequency of extratropical cyclones decreases in UC, USE1 and USE2, which may be partly responsible for the decrease in their mean values of SRH1 and SHR6 from spring to summer.

Examples of the most common patterns observed in JS (Figure S3a), UC (Figure S4a), USE1 (Figure S5a) and USE2 (Figure S6a) were selected to further investigate their detailed differences in environmental features at different levels (Figures 11 and S7). JS was influenced by a deep trough to the west and a subtropical high to the east in the middle troposphere, with synoptic-scale southwesterly flows in the lower troposphere. The values of SHR6 were generally small in JS. The strong southwesterly flows enhanced the northeastward transport of moisture from the south to JS as well as enhancing the low-level wind speed, which was favourable for the development of instability and large SRH1 values (Figure S7i,e). However, the region with a good configuration of kinematic and thermodynamic conditions with a high STP value was limited to only a small area near JS (Figure S7m). In contrast, in the cases of the US locations, intense surface cyclones with strong upper-level jets produced large areas with strong vertical wind shear and low-level storm relative helicity (Figure S7). In addition, the UC region was

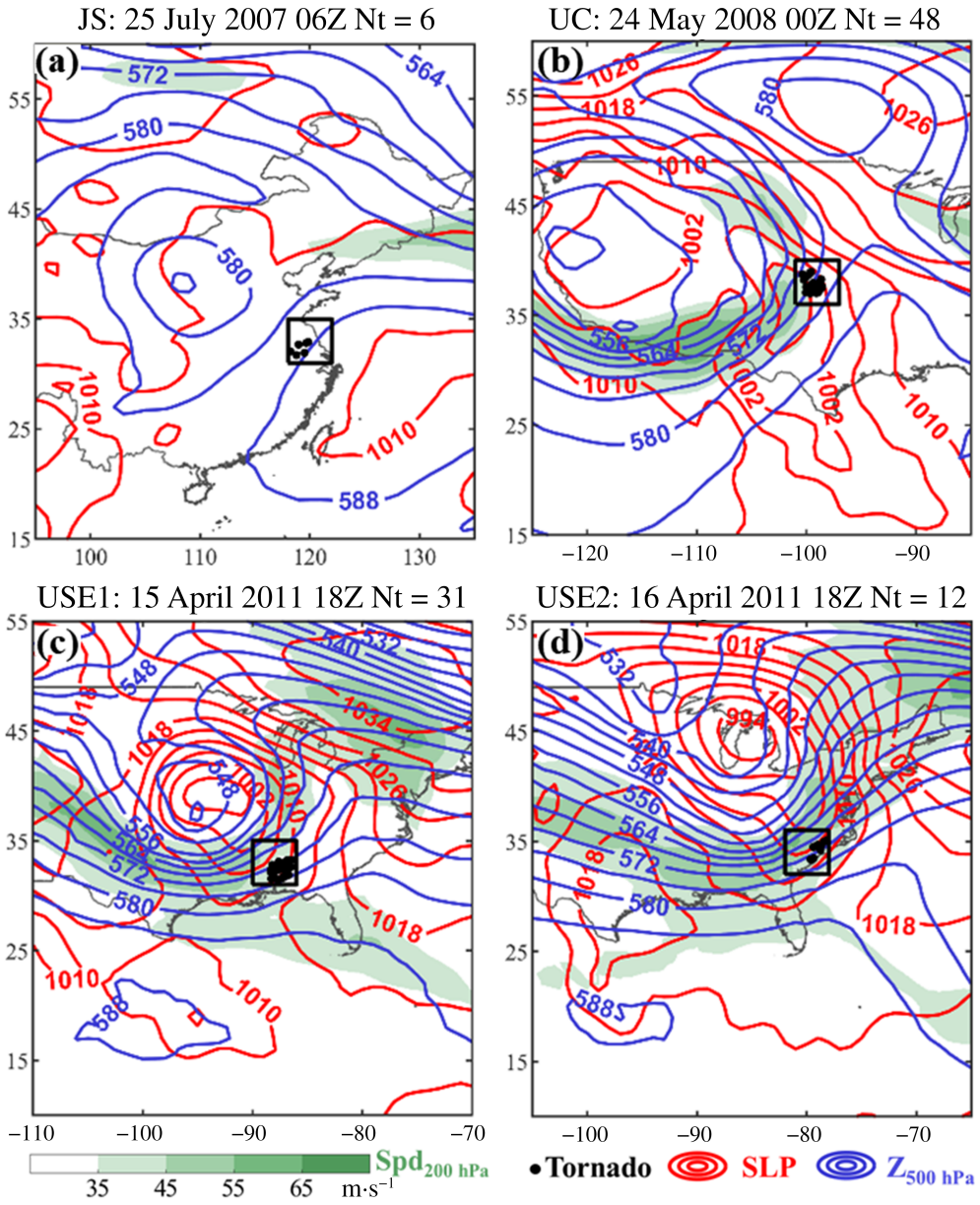

FIGURE 11 Examples of the synoptic situations of typical high-Nt tornado events in JS (a), UC (b), USE1 (c), and USE2 (d), including the geopotential heights (blue contours; 10 gpm) at 500 hPa, sea level pressure (red contours; hPa) and the wind speeds greater than 35 m s^{-1} at 200 hPa (shading, m s^{-1}). The locations of tornadoes are denoted by black dots and the target regions are indicated by black boxes. The time of NCEP FNL data, determined as the closest time before the mean time of occurrences of all tornadoes of the corresponding tornado event, has been labelled at the top of the corresponding panel

controlled by a long dryline and accompanied by a southerly jet at 925 hPa (Figure S7j). Dry air from the western highlands was advected over warm humid air from the Gulf of Mexico, producing a large area with high potential instability and convergence for convection initiation. The better match of the kinematic and thermodynamic parameters in UC and the more favourable kinematic conditions in USE1 and USE2, helped produce wider areas with higher STP values than those in JS (Figure S7). These high-STP areas were favourable for triggering widespread tornado outbreaks.

The tornado-generating efficiency of tornado events is also greatly influenced by the convective modes of the parent storms. Relative to all other non-supercell convective modes, supercell systems were found to be more productive of tornadoes (Duda and Gallus, 2010). Smith *et al.* (2012) showed that the ratio of non-supercell tornadoes to supercell tornadoes could differ among different regions, and the estimated percentage of right-moving supercell tornadoes was greater than 80% in UC and greater than 70% in USE1 and USE2. Compared with the target regions in the United States, JS features much weaker ambient environment shear during its tornado season, which is unfavourable for the development of supercells. The proportion of supercell tornadoes in JS is probably lower than those in UC, USE1 and USE2. The detailed statistical characteristics of convective modes that are conducive to tornadoes in China remain unclear and are worth exploring in future research.

In addition, this study only focuses on tornado-prone regions and on the prime months of tornado occurrence in the two studied countries; the environmental

differences obtained herein cannot be extrapolated to all areas in either country. Tornado activities and tornado-related environmental parameters have obvious regional differences and seasonal variations. For example, the tornado-prone region in the southern part of China, which is located in Guangdong Province and labelled GD (a 4° × 4° area within 21–25°N and 111–115°E, as shown in Figure S1a), has a springtime tornado peak (Figure S1b,c). The evolutions of SHR6, SRH1, MLCAPE and STP in GD are quite close to those observed in USE1 rather than in JS (Figure S2). MLCAPE increases much earlier in GD than in JS. A good match between MLCAPE and SHR6 occurs during the stage when SRH6 is still quite large. In addition, GD is characterized by lower MLLCL values than all four other target regions (Figure S2). These environmental features should have produced a high frequency of tornadoes and a high tornado-generating efficiency of tornado events in GD, as those observed in USE1. However, GD even has far fewer tornadoes than JS, possibly because of its mountainous topography. In contrast, most areas in the JS region are plains (Figure S1a), and the good match between SHR6 and MLCAPE occurs during a stage in which the SHR6 values have already largely decreased due to the higher latitude of JS than that of GD.

As observed in GD, terrain may have an important impact on the differences in tornado activities between the United States and China. Previous statistical analyses over the Great Plains and Arkansas have shown that terrain roughness has a negative effect on the tornado probability at a fixed population density (Jagger *et al*., 2015; Elsner *et al*., 2016; Hua and Chavas, 2019). China has fairly mountainous regions in the south, from Guangdong to Zhejiang Provinces. Similar to the United States, most tornadoes in China also occur in plains (Figure S1). Consequently, far fewer tornadoes are possibly to occur in China than in the United States because there are many fewer plains in China, and the only large-extent plain area is located farther to the north and is characterized by an unfavourable kinematic environment for tornado occurrences during the tornado season.

Finally, it should be mentioned that there is still some room for improvement in this study, but unfortunately, it is difficult to improve this study due to the limitations of tornado data in China. Relative to the currently used 10-year tornado records, a longer study period should yield results that are closer to the nature of the relationship between the tornado numbers and environmental parameters. Since a 10-year period is not sufficiently long to eliminate the effects of statistical noise, it is difficult to define a precise 90-day peak season. If a longer-term tornado database were available in China, defining the tornado season as a consecutive 90-day period rather than as three calendar months, as was done in this study, might more precisely represent the peak tornado occurrences. In addition, it is inevitable that some tornadoes are not detected and recorded, especially weak tornadoes occurring in rural areas with low population densities. However, based on version 4 of the Columbia University Gridded Population of the World dataset (Center for International Earth Science Information Network—CIESIN—Columbia University, 2016), eastern and southern China are much more densely populated than the central and southeastern United States. Consequently, the missing records in JS and GD could thus be at least close to those in UC, USE1 and USE2. This limitation should not affect the main findings in this study.

5 | SUMMARY

This study was aimed at understanding the substantial differences in the tornado frequency and tornado season timing between China and the United States by comparing the key tornado-associated environmental features in the high-incidence regions.

The results show that the much higher potential in the occurrence of multiple tornadoes over a short period is probably responsible for the larger tornado numbers recorded in the United States than in China. During the earlier tornado season, the target regions in the United States have apparently higher tornado-generating efficiencies of tornado events than the JS region of China. In the target regions of the United States, the decrease in tornado-generating efficiency from spring to summer is possibly due in part to the decreases in the SRH1 and SHR6 values.

The results also show that the STP has a better correlation with tornado activity than do individual kinematic or thermodynamic parameters. The STP averages show a monotonic decrease with the decrease in the area-scaled total tornado count from UC to USE1, JS, and USE2 during their respective tornado seasons. For a given region, the month with the maximum mean STP value is also the month with peak tornado occurrences. Compared with the target regions in the United States, the JS in China reaches the peak STP in a later month and thus has a delayed tornado season.

Compared with the JS region in China, the target regions in the United States have more favourable kinematic environments for supercells, with much higher SHR6 values. One interesting finding is that this is not because SHR6 is generally larger in the United States than that in China at any time of the year. The target regions in the United States actually have mean values and decreasing trends of SHR6 from spring to summer

that are similar to those in the JS region of China. However, the United States regions have much earlier increases in instability than the JS region of China, resulting in an earlier good match between SHR6 and MLCAPE and thus a higher SHR6 value during their earlier tornado seasons. These environmental features may have resulted from the weaker, less frequent, and more northern upper-level jet streams and extratropical cyclones in the tornado seasons of JS than their counterparts in the United States.

ACKNOWLEDGEMENTS

This work was supported by the National Natural Science Foundation of China (Grant 41875051, 41905043 and 42030604). We thank Yipeng Huang (Xiamen Meteorological Bureau, China) for his constructive comments. We also thank the anonymous reviewers for their insightful comments in improving our work.

AUTHOR CONTRIBUTIONS

Ruilin Zhou: Data curation; formal analysis; investigation; methodology; software; validation; visualization; writing-original draft; writing-review & editing. **Zhiyong Meng:** Conceptualization; formal analysis; funding acquisition; investigation; methodology; project administration; resources; supervision; visualization; writing-review & editing. **Lanqiang Bai:** Formal analysis; funding acquisition; investigation; software; writing-review & editing.

ORCID

Ruilin Zhou https://orcid.org/0000-0003-1257-9980
Zhiyong Meng https://orcid.org/0000-0002-2527-1056
Lanqiang Bai https://orcid.org/0000-0002-0304-5656

REFERENCES

Anderson-Frey, A.K., Richardson, Y.P., Dean, A.R., Thompson, R. L. and Smith, B.T. (2016) Investigation of near-storm environments for tornado events and warnings. *Weather and Forecasting*, 31(6), 1771–1790. https://doi.org/10.1175/waf-d-16-0046.1.

Anderson-Frey, A.K., Richardson, Y.P., Dean, A.R., Thompson, R. L. and Smith, B.T. (2018) Near-storm environments of outbreak and isolated tornadoes. *Weather and Forecasting*, 33(5), 1397–1412. https://doi.org/10.1175/waf-d-18-0057.1.

Ashley, W.S. (2007) Spatial and temporal analysis of tornado fatalities in the United States: 1880–2005. *Weather and Forecasting*, 22(6), 1214–1228. https://doi.org/10.1175/2007waf2007004.1.

Bai, L., Meng, Z., Sueki, K., Chen, G. and Zhou, R. (2020) Climatology of tropical cyclone tornadoes in China from 2006 to 2018. *Science China Earth Sciences*, 63(1), 37–51. https://doi.org/10.1007/s11430-019-9391-1.

Brooks, H.E. (2009) Proximity soundings for severe convection for Europe and the United States from reanalysis data. *Atmospheric Research*, 93(1–3), 546–553. https://doi.org/10.1016/j.atmosres.2008.10.005.

Brooks, H.E., Lee, J.W. and Craven, J.P. (2003) The spatial distribution of severe thunderstorm and tornado environments from global reanalysis data. *Atmospheric Research*, 67–68, 73–94. https://doi.org/10.1016/s0169-8095(03)00045-0.

Brown, M.C. and Nowotarski, C.J. (2020) Southeastern U.S. tornado outbreak likelihood using daily climate indices. *Journal of Climate*, 33(8), 3229–3252. https://doi.org/10.1175/jcli-d-19-0684.1.

Bunkers, M.J., Klimowski, B.A., Zeitler, J.W., Thompson, R.L. and Weisman, M.L. (2000) Predicting supercell motion using a new hodograph technique. *Weather and Forecasting*, 15(1), 61–79. https://doi.org/10.1175/1520-0434(2000)015<0061:Psmuan>2.0.Co;2.

Center for International Earth Science Information Network—CIESIN—Columbia University. (2016) *Gridded Population of the World, Version 4 (GPWv4): Population Density*. Palisades, NY: NASA Socioeconomic Data and Applications Center (SEDAC). https://doi.org/10.7927/H4NP22DQ.

Chen, J., Cai, X., Wang, H., Kang, L., Zhang, H., Song, Y., Zhu, H., Zheng, W. and Li, F. (2018) Tornado climatology of China. *International Journal of Climatology*, 38(5), 2478–2489. https://doi.org/10.1002/joc.5369.

China Meteorological Administration. (2005–2017) *Yearbook of Meteorological Disasters in China (in Chinese)*. Beijing: China Meteorological Press.

Coffer, B.E., Parker, M.D., Thompson, R.L., Smith, B.T. and Jewell, R.E. (2019) Using near-ground storm relative helicity in supercell tornado forecasting. *Weather and Forecasting*, 34(5), 1417–1435. https://doi.org/10.1175/waf-d-19-0115.1.

Coleman, T.A. and Dixon, P.G. (2014) An objective analysis of tornado risk in the United States. *Weather and Forecasting*, 29(2), 366–376. https://doi.org/10.1175/Waf-D-13-00057.1.

Davies-Jones, R. (2015) A review of supercell and tornado dynamics. *Atmospheric Research*, 158–159, 274–291. https://doi.org/10.1016/j.atmosres.2014.04.007.

Davies-Jones, R.P., Burgess, D.W. and Foster, M.P. (1990) Test of helicity as a tornado forecast parameter. *Preprints, 16th Conf. on Severe Local Storms*, 588–592.

Duda, J.D. and Gallus, W.A. (2010) Spring and summer midwestern severe weather reports in supercells compared to other morphologies. *Weather and Forecasting*, 25(1), 190–206. https://doi.org/10.1175/2009waf2222338.1.

Elsner, J.B., Fricker, T., Widen, H.M., Castillo, C.M., Humphreys, J., Jung, J., Rahman, S., Richard, A., Jagger, T.H., Bhatrasataponkul, T., Gredzens, C. and Dixon, P.G. (2016) The relationship between elevation roughness and tornado activity: a spatial statistical model fit to data from the central Great Plains. *Journal of Applied Meteorology and Climatology*, 55(4), 849–859. https://doi.org/10.1175/jamc-d-15-0225.1.

Emanuel, K.A. (1994) *Atmospheric Convection*. New York: Oxford University Press.

Fan, W. and Yu, X. (2015) Characteristics of spatial-temporal distribution of tornadoes in China (in Chinese with English abstract). *Meteorological Monthly*, 41(7), 793–805.

Farney, T.J. and Dixon, P.G. (2015) Variability of tornado climatology across the continental United States. *International Journal of Climatology*, 35(10), 2993–3006. https://doi.org/10.1002/joc.4188.

Feng, Z., Houze, R.A., Leung, L.R., Song, F., Hardin, J.C., Wang, J., Gustafson, W.I. and Homeyer, C.R. (2019) Spatiotemporal characteristics and large-scale environments of mesoscale convective

systems east of the Rocky mountains. *Journal of Climate*, 32(21), 7303–7328. https://doi.org/10.1175/jcli-d-19-0137.1.

Galway, J.G. (1977) Some climatological aspects of tornado outbreaks. *Monthly Weather Review*, 105(4), 477–484. https://doi.org/10.1175/1520-0493(1977)105<0477:Scaoto>2.0.Co;2.

Gensini, V.A. and Bravo De Guenni, L. (2019) Environmental covariate representation of seasonal U.S. tornado frequency. *Journal of Applied Meteorology and Climatology*, 58(6), 1353–1367. https://doi.org/10.1175/jamc-d-18-0305.1.

Gensini, V.A. and Brooks, H.E. (2018) Spatial trends in United States tornado frequency. *NPJ Climate and Atmospheric Science*, 1(1), 1–5. https://doi.org/10.1038/s41612-018-0048-2.

Glickman, T.S. (2000) *Glossary of Meteorology*. Boston: American Meteorological Society.

Grams, J.S., Thompson, R.L., Snively, D.V., Prentice, J.A., Hodges, G.M. and Reames, L.J. (2012) A climatology and comparison of parameters for significant tornado events in the United States. *Weather and Forecasting*, 27(1), 106–123. https://doi.org/10.1175/waf-d-11-00008.1.

Grünwald, S. and Brooks, H.E. (2011) Relationship between sounding derived parameters and the strength of tornadoes in Europe and the USA from reanalysis data. *Atmospheric Research*, 100 (4), 479–488. https://doi.org/10.1016/j.atmosres.2010.11.011.

Hart, J.A. and Korotky, W. (1991) The SHARP workstation v1.50 users guide. NOAA/National Weather Service, 30 pp. [Available from NWS Eastern Region Headquarters, 630 Johnson Ave., Bohemia, NY 11716.]

Hua, Z. and Chavas, D.R. (2019) The empirical dependence of tornadogenesis on elevation roughness: historical record analysis using Bayes's law in Arkansas. *Journal of Applied Meteorology and Climatology*, 58(2), 401–411. https://doi.org/10.1175/jamc-d-18-0224.1.

Jagger, T.H., Elsner, J.B. and Widen, H.M. (2015) A statistical model for regional tornado climate studies. *PLoS One*, 10(8), e0131876. https://doi.org/10.1371/journal.pone.0131876.

Kendall, M. and Gibbons, J.D. (1990) *Rank Correlation Methods*. London: Edward Arnold.

Kerr, B.W. and Darkow, G.L. (1996) Storm-relative winds and helicity in the tornadic thunderstorm environment. *Weather and Forecasting*, 11(4), 489–505. https://doi.org/10.1175/1520-0434(1996)011<0489:Srwahi>2.0.Co;2.

Landsea, C.W. and Franklin, J.L. (2013) Atlantic hurricane database uncertainty and presentation of a new database format. *Monthly Weather Review*, 141(10), 3576–3592. https://doi.org/10.1175/mwr-d-12-00254.1.

Lee, J., Son, S.-W., Cho, H.-O., Kim, J., Cha, D.-H., Gyakum, J.R. and Chen, D. (2019) Extratropical cyclones over East Asia: climatology, seasonal cycle, and long-term trend. *Climate Dynamics*, 54(1–2), 1131–1144. https://doi.org/10.1007/s00382-019-05048-w.

Long, J.A., Stoy, P.C. and Gerken, T. (2018) Tornado seasonality in the southeastern United States. *Weather and Climate Extremes*, 20, 81–91. https://doi.org/10.1016/j.wace.2018.03.002.

Lu, M., Tippett, M. and Lall, U. (2015) Changes in the seasonality of tornado and favorable genesis conditions in the Central United States. *Geophysical Research Letters*, 42(10), 4224–4231. https://doi.org/10.1002/2015gl063968.

Manney, G.L., Hegglin, M.I., Daffer, W.H., Schwartz, M.J., Santee, M.L. and Pawson, S. (2014) Climatology of upper tropospheric–lower stratospheric (UTLS) jets and tropopauses in MERRA. *Journal of Climate*, 27(9), 3248–3271. https://doi.org/10.1175/jcli-d-13-00243.1.

Markowski, P.M. and Richardson, Y.P. (2010) *Organization of Isolated Convection. Mesoscale Meteorology in Midlatitudes*. Chichester: John Wiley.

Markowski, P.M. and Richardson, Y.P. (2014) The influence of environmental low-level shear and cold pools on tornadogenesis: insights from idealized simulations. *Journal of the Atmospheric Sciences*, 71(1), 243–275. https://doi.org/10.1175/jas-d-13-0159.1.

Mccaul, E.W. (1991) Buoyancy and shear characteristics of hurricane-tornado environments. *Monthly Weather Review*, 119 (8), 1954–1978. https://doi.org/10.1175/1520-0493(1991)119<1954:Bascoh>2.0.Co;2.

Mercer, A.E., Shafer, C.M., Doswell, C.A., Leslie, L.M. and Richman, M.B. (2012) Synoptic composites of tornadic and nontornadic outbreaks. *Monthly Weather Review*, 140(8), 2590–2608. https://doi.org/10.1175/mwr-d-12-00029.1.

Molina, M.J. and Allen, J.T. (2019) On the moisture origins of tornadic thunderstorms. *Journal of Climate*, 32(14), 4321–4346. https://doi.org/10.1175/jcli-d-18-0784.1.

Nowotarski, C.J. and Jensen, A.A. (2013) Classifying proximity soundings with self-organizing maps toward improving supercell and tornado forecasting. *Weather and Forecasting*, 28 (3), 783–801. https://doi.org/10.1175/waf-d-12-00125.1.

Potvin, C.K., Elmore, K.L. and Weiss, S.J. (2010) Assessing the impacts of proximity sounding criteria on the climatology of significant tornado environments. *Weather and Forecasting*, 25 (3), 921–930. https://doi.org/10.1175/2010waf2222368.1.

Rasmussen, E.N. (2003) Refined supercell and tornado forecast parameters. *Weather and Forecasting*, 18(3), 530–535. https://doi.org/10.1175/1520-0434(2003)18<530:Rsatfp>2.0.Co;2.

Rasmussen, E.N. and Blanchard, D.O. (1998) A baseline climatology of sounding-derived supercell and tornado forecast parameters. *Weather and Forecasting*, 13(4), 1148–1164. https://doi.org/10.1175/1520-0434(1998)013<1148:Abcosd>2.0.Co;2.

Sherburn, K.D. and Parker, M.D. (2014) Climatology and ingredients of significant severe convection in high-shear, low-CAPE environments. *Weather and Forecasting*, 29(4), 854–877. https://doi.org/10.1175/waf-d-13-00041.1.

Smith, B.T., Thompson, R.L., Grams, J.S., Broyles, C. and Brooks, H.E. (2012) Convective modes for significant severe thunderstorms in the contiguous United States. Part I: storm classification and climatology. *Weather and Forecasting*, 27(5), 1114–1135. https://doi.org/10.1175/waf-d-11-00115.1.

Tang, Y., Xu, X., Xue, M., Tang, J. and Wang, Y. (2020) Characteristics of low-level meso-γ-scale vortices in the warm season over East China. *Atmospheric Research*, 235, 104768. https://doi.org/10.1016/j.atmosres.2019.104768.

Taszarek, M., Brooks, H.E. and Czernecki, B. (2017) Sounding-derived parameters associated with convective hazards in europe. *Monthly Weather Review*, 145(4), 1511–1528. https://doi.org/10.1175/mwr-d-16-0384.1.

Thompson, R.L., Edwards, R., Hart, J.A., Elmore, K.L. and Markowski, P. (2003) Close proximity soundings within supercell environments obtained from the rapid update cycle. *Weather and Forecasting*, 18(6), 1243–1261. https://doi.org/10.1175/1520-0434(2003)018<1243:Cpswse>2.0.Co;2.

Thompson, R.L., Smith, B.T., Grams, J.S., Dean, A.R. and Broyles, C. (2012) Convective modes for significant severe thunderstorms in the contiguous United States. Part II: Supercell and QLCS tornado environments. *Weather and Forecasting*, 27 (5), 1136–1154. https://doi.org/10.1175/waf-d-11-00116.1.

Tippett, M.K., Sobel, A.H. and Camargo, S.J. (2012) Association of U.S. tornado occurrence with monthly environmental parameters. *Geophysical Research Letters*, 39(2), L02801. https://doi.org/10.1029/2011gl050368.

Tippett, M.K., Sobel, A.H., Camargo, S.J. and Allen, J.T. (2014) An empirical relation between U.S. tornado activity and monthly environmental parameters. *Journal of Climate*, 27(8), 2983–2999. https://doi.org/10.1175/Jcli-D-13-00345.1.

Tochimoto, E. and Niino, H. (2016) Structural and environmental characteristics of extratropical cyclones that cause tornado outbreaks in the warm sector: a composite study. *Monthly Weather Review*, 144(3), 945–969. https://doi.org/10.1175/mwr-d-15-0015.1.

Wernli, H. and Schwierz, C. (2006) Surface cyclones in the ERA-40 dataset (1958–2001). Part I: novel identification method and global climatology. *Journal of the Atmospheric Sciences*, 63(10), 2486–2507. https://doi.org/10.1175/jas3766.1.

Zhou, R., Meng, Z. and Bai, L. (2020). Tornado database in China (2007∼2016). V2 ed.: Peking University Open Research Data Platform. https://doi.org/10.18170/DVN/QKQHTG.

SUPPORTING INFORMATION

Additional supporting information may be found online in the Supporting Information section at the end of this article.

How to cite this article: Zhou, R., Meng, Z., & Bai, L. (2022). Differences in tornado activities and key tornadic environments between China and the United States. *International Journal of Climatology*, *42*(1), 367–384. https://doi.org/10.1002/joc.7248